Optical properties of coupled metal-semiconductor and metal-molecule nanocrystal complexes: Role of multipole effects

Jie-Yun Yan,[1,2] Wei Zhang,[1,*] Suqing Duan,[1] Xian-Geng Zhao,[1] and Alexander O. Govorov[3,†]
[1]*Institute of Applied Physics and Computational Mathematics, P.O. Box 8009, Beijing 100088, People's Republic of China*
[2]*Department of Physics, Tsinghua University, Beijing 100084, People's Republic of China*
[3]*Department of Physics and Astronomy, Ohio University, Athens, Ohio 45701-2979, USA*
(Received 19 January 2008; published 1 April 2008)

We theoretically investigate the effects of interaction between an optical dipole (semiconductor quantum dot or molecule) and metal nanoparticles. The calculated absorption spectra of hybrid structures demonstrate strong effects of interference coming from the exciton-plasmon coupling. In particular, the absorption spectra acquire characteristic asymmetric line shapes and strong antiresonances. We present here an exact solution of the problem beyond the dipole approximation and find that the multipole treatment of the interaction is crucial for the understanding of strongly interacting exciton-plasmon nanosystems. Interestingly, the visibility of the exciton resonance becomes greatly enhanced for small interparticle distances due to the interference phenomenon, multipole effects, and electromagnetic enhancement. We find that the destructive interference is particularly strong. Using our exact theory, we show that the interference effects can be experimentally observed in the exciting systems even at room temperature.

DOI: 10.1103/PhysRevB.77.165301 PACS number(s): 71.35.Cc, 73.21.La, 73.90.+f

I. INTRODUCTION

Nanomaterials incorporating semiconductor quantum dots (SQDs), metal nanoparticles (MNPs), metal surfaces, and dye molecules have been intensively studied.[1–13] Such hybrid structures take advantage of physical properties of different material systems and demonstrate useful sensor and light-harvesting properties. In a complex made of an emitter (SQD or dye) and MNPs, excitons and plasmons interact via the Coulomb forces. Emission of SQD (dye) in the presence of MNPs can be suppressed or enhanced depending on the size and organization of the nanoassembly.[3,5,11] This occurs due to the following physical factors: (1) modified density of states of photons, (2) amplified absorption in the presence of plasmon resonance in the MNPs, and (3) shortening of exciton lifetime due to an increased radiation rate and energy transfer to the MNPs. Theoretically, an emitting dipole in the vicinity of metal objects has been studied in many publications.[3,5,11–14] The exciton-plasmon interaction between an emitting dipole and metal objects leads to energy transfer, a shift of energy of the quantum emitter, and vacuum Rabi oscillations.[11–14] The energy transfer mechanism is similar to Förster transfer between two dye molecules.[15] In most theoretical publications, the energy transfer in nanoscale systems was treated as unidirectional flow of energy from a donor to an accepter using the rate equations. This rate-equation approach describes noncoherent interactions at elevated temperatures. Very recently, several theoretical studies were performed for the quantum regime of exciton-plasmon interaction between a SQD/dye and MNP.[16–19] These studies revealed a novel feature of strongly interacting hybrid nanocrystals—interference effects. The absorption spectra of coupled SQD and MNP acquire characteristic asymmetry due to the interference of external and induced electric fields. At low temperatures and small exciton broadening, the absorption line shapes are described by the Fano formula.[20] However, previous theoretical results[16–19] were based on the dipole approximation. The dipole approximation is valid when an exciton-MNP distance is large, compared to the sizes of components, and the exciton-plasmon interaction is relatively weak. However, the most interesting regime of strong exciton-plasmon interaction appears when an exciton-MNP distance is small and the dipole approximation is not valid anymore. Therefore, to describe the regime of strong exciton-plasmon coupling, one should exactly treat the Coulomb interaction, including electric multipole effects. In this paper, we obtain an exact solution for the problem of an interacting dipole and MNP.

Here, we present a theory of strong exciton-plasmon interaction and show that the multipole effects are of crucial importance for the understanding of the exciton-plasmon interaction in the most interesting regime of small exciton-MNP separations. A strong interaction between excitons and plasmons at small exciton-MNP distances reveals itself in absorption spectra as asymmetric line shapes and antiresonances (deep minima). Moreover, we consider two types of nanoscale hybrid complexes (SQD-MNP and dye-MNP) and show that, for small exciton-MNP distances, the interference effects can appear in room-temperature experiments. For the multipole regime of Coulomb interaction, the visibility of exciton resonance dramatically grows due to both the interference effect and the plasmon-induced electromagnetic enhancement. For large interparticle distances, the absorptions by a SQD and MNP constructively add up. For the hybrid structures of small dimensions, the spectra exhibit very strong effects of constructive and destructive interferences. We think that these interference effects can be experimentally observed by using the present available material systems.

In this paper, we discuss three material systems: colloidal nanocrystals, self-assembled dots, and dye molecules. Most of the current experiments on metal-semiconductor and metal-dye assemblies employ colloidal nanoparticles[5–9] and nanowires.[6] To observe the effects described in this paper,

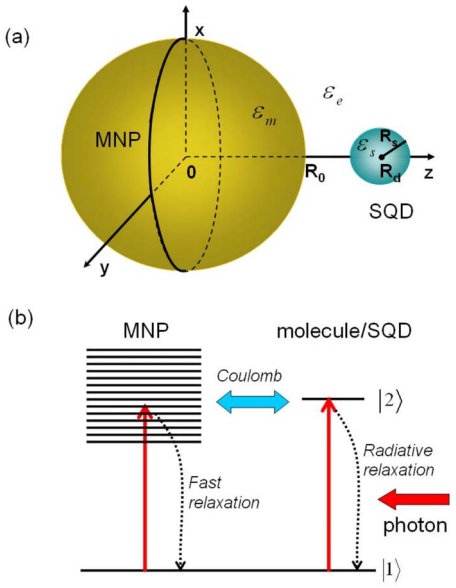

FIG. 1. (Color online) (a) The model of semiconductor-metal nanoparticle molecule. (b) The energy structure of the system; the arrows describe the main transitions.

single colloidal nanocrystal complexes can be deposited on a surface or buried in a polymer film. Assembly measurements of colloidal complexes in a solution can also be suitable. Presently, there are attempts to fabricate metal nanoparticles inside epitaxial structures.[21] Potentially, colloidal and epitaxial nanocrystals can be combined in one structure.[22] For example, an epitaxial dot can be buried close to the surface[23] and a MNP can be attached to the surface.

The paper is organized as follows. In Sec. II, we give a description of the electric field inside the system. The optical properties of a nanocrystal molecule are presented in Sec. III. Section IV discusses the absorption line shape. The numerical results for SQD-MNP molecules and dye molecule-MNP nanocrystals are given in Sec. V. Finally, a brief conclusion is presented in Sec. VI.

II. ELECTRIC FIELDS INSIDE THE SYSTEM

Now, we consider the hybrid nanocrystal molecule composed of a spherical MNP of radius R_0 and a spherical SQD of radius R_s in the environment with dielectric constant ε_e [see Fig. 1(a)]. The center-to-center distance for the nanocrystals is denoted as R_d. In the following, we will assume that a SQD has small dimensions $R_s \ll R_d$, whereas the size of the MNP can be arbitrary, i.e., $R_0 \sim R_d$. In the case of a dye molecule-MNP complex, the size R_d becomes irrelevant and we have only the obvious condition: the molecule-MNP distance R_d should be larger than the MNP radius, i.e., $R_d > R_0$.

When the hybrid molecule (SQD-MNP or dye-MNP) is radiated with a laser, the oscillating electric field excites both the interband transition in a SQD and the plasmon in a MNP. The interband transition (exciton) in a SQD (dye) has an oscillating dipole moment and, therefore, creates an oscillating electric field that acts on a MNP and excites the plasmons. The plasmons excited in a MNP in turn influence the exciton. In this way, the exciton and plasmon form a new collective excitation—a hybrid exciton. The origin of this hybrid exciton is in the Coulomb interaction between a SQD and MNP [Fig. 1(b)].

Since a nanoscale structure has small dimensions, we assume that the electric field of the laser is spatially uniform and use the quasistatic approximation. Also, we describe the MNP with the local dynamic dielectric function $\varepsilon_m(\omega)$. By carefully solving Laplace's equation $\nabla^2\varphi=0$, we can get the electric potential φ and the electric field $\boldsymbol{E}=-\nabla\varphi$. As for the dipole in the SQD, we take it as a perfect dipole, labeled as $\boldsymbol{p}$, because the radius of SQD R_s is much smaller in contrast with R_0 usually.

We now consider the laser electric field in the form $\boldsymbol{E}_0(t)=\tilde{\boldsymbol{E}}_0 \cos \omega t$. We first discuss the part with positive frequency, $\tilde{\boldsymbol{E}}_0 e^{-i\omega t}/2$. The electric field inside a SQD could be split into three parts: $\boldsymbol{E}_{\mathrm{SQD}}=(\tilde{\boldsymbol{E}}_1+\tilde{\boldsymbol{E}}_2+\tilde{\boldsymbol{E}}_3)e^{-i\omega t}$. $\tilde{\boldsymbol{E}}_1 e^{-i\omega t}$ is the electric field induced by $\boldsymbol{E}_0$ inside a SQD in the absence of a MNP,[24]

$$\tilde{\boldsymbol{E}}_1 = \frac{\varepsilon_e}{\varepsilon_{\mathrm{eff1}}}\frac{\tilde{\boldsymbol{E}}_0}{2}, \tag{1}$$

where $\varepsilon_{\mathrm{eff1}}=(\varepsilon_s+2\varepsilon_e)/3$ is the effective dielectric constant of the SQD and ε_s is the background dielectric constant of the semiconductor.

The second part $\tilde{\boldsymbol{E}}_2 e^{-i\omega t}$ comes from surface charges of a MNP induced only by the external optical electric field $\tilde{\boldsymbol{E}}_0 e^{-i\omega t}/2$,

$$\tilde{\boldsymbol{E}}_2 = s_\alpha \frac{\varepsilon_e \gamma_1 R_0^3}{\varepsilon_{\mathrm{eff1}} R_d^3}\frac{\tilde{\boldsymbol{E}}_0}{2}, \tag{2}$$

where $\gamma_1=[\varepsilon_m(\omega)-\varepsilon_e]/[\varepsilon_m(\omega)+2\varepsilon_e]$ and $s_\alpha=2\,(-1)$ for electric field polarization $\boldsymbol{E}_0$ is parallel to the z (x) axis. The choice of a sign of the imaginary part of the dielectric constant should be the following: $\mathrm{Im}[\varepsilon_m(\omega)]>0$ if $\omega>0$.

The last part $\tilde{\boldsymbol{E}}_3 e^{-i\omega t}$ is the SQD-felt effective electric field produced by the multipole polarization in a MNP induced by the effective dipole of a SQD $\boldsymbol{p}(t)=(\varepsilon_e/\varepsilon_{\mathrm{eff1}})\tilde{\boldsymbol{p}}e^{-i\omega t}$. This part is the most important one, underlying the interaction of the MNP and SQD. We finally find that this part of the electric field is

$$\tilde{\boldsymbol{E}}_3 = \sum_{n=1}^{\infty} \frac{s_n \varepsilon_e \gamma_n R_0^{2n+1}}{\varepsilon_{\mathrm{eff1}}^2 R_d^{2n+4}}\tilde{\boldsymbol{p}}, \tag{3}$$

where

$$\gamma_n = \frac{\varepsilon_m(\omega)-\varepsilon_e}{\varepsilon_m(\omega)+\dfrac{n+1}{n}\varepsilon_e}, \tag{4}$$

and the coefficient $s_n=(n+1)^2$ or $P_n'(1)$ for the polarization $\boldsymbol{p}$ parallel to the z or x axis, respectively. Here, P_n is the Legendre function and $P_n'(1)$ is the differential of Legendre function at the argument of 1.

When $n=1$, the electric field $\tilde{\boldsymbol{E}}_3$ becomes

$$\tilde{\boldsymbol{E}}_3 = s_1 \frac{\gamma_1 \varepsilon_e R_0^3}{\varepsilon_{\text{eff}1}^2 R_d^6} \tilde{\boldsymbol{p}}, \tag{5}$$

which is the result under the dipole approximation: the SQD dipole-induced electric field everywhere inside the MNP is uniform and equals to the value at the center of the MNP. This dipole approximation is used in Ref. 16, which is reasonable when the distance R_d is relatively large because the factor $1/R_d^{2n+4}$ makes other terms negligible. However, when the distance is comparable to the radius of MNP, i.e., $R_0 \sim R_d$, which is always the case in such molecules, the items $n>1$ become important and may even have a bigger contribution than the leading terms. Actually, the items with different n are related to different order multipole polarization in MNP: $n=1$ is dipole, $n=2$ quadrupole, $n=3$ octopole, and so on. The function of γ_n [Eq. (4)] also reflects the characteristics of the multipole polarization, as reported by the Mie theory.[25,26] However, it should be noticed that the multipole effect in Mie theory is caused by the comparable radius of the MNP with wavelength of the light. Here, the radius is small enough to neglect the effect and hence the multipole effect totally comes from the induced polarization by the SQD when the interparticle distance is relatively small.

The electric field inside MNP $\boldsymbol{E}_{\text{MNP,tot}}(t)$ can also be solved, and the corresponding positive frequency part is $\tilde{\boldsymbol{E}}_{\text{MNP,tot}} e^{-i\omega t} = (\frac{\varepsilon_e}{\varepsilon_{\text{eff}2}} \frac{\tilde{\boldsymbol{E}}_0}{2} + \tilde{\boldsymbol{E}}_{\text{MNP}}) e^{-i\omega t}$, where $\varepsilon_{\text{eff}2} = [\varepsilon_m(\omega) + 2\varepsilon_e]/3$ and $\tilde{\boldsymbol{E}}_{\text{MNP}}$ is

$$\tilde{\boldsymbol{E}}_{\text{MNP}}|_{\boldsymbol{E}\parallel\hat{\boldsymbol{z}}} = \sum_{n=1}^{\infty} \frac{(n+1)\beta_n R^{n-1} |\tilde{\boldsymbol{p}}|}{\varepsilon_{\text{eff}\,1} R_d^{n+2}} \times \left[-\frac{x\hat{\boldsymbol{x}} + y\hat{\boldsymbol{y}}}{R} P'_{n-1}(z/R) + n P_{n-1}(z/R)\hat{\boldsymbol{z}} \right], \tag{6}$$

$$\tilde{\boldsymbol{E}}_{\text{MNP}}|_{\boldsymbol{E}\parallel\hat{\boldsymbol{x}}} = \sum_{n=1}^{\infty} \frac{\beta_n R^{n-1} |\tilde{\boldsymbol{p}}|}{\varepsilon_{\text{eff}\,1} R_d^{n+2}} \left\{ \left[-nP_{n-1}(z/R) - \frac{z}{R} P'_{n-1}(z/R) + \frac{x^2}{R^2} P''_{n-1}(z/R) \right] \hat{\boldsymbol{x}} + \frac{xy}{R^2} P''_{n-1}(z/R)\hat{\boldsymbol{y}} - (n+1)\frac{x}{R} P'_{n-1}(z/R)\hat{\boldsymbol{z}} \right\}, \tag{7}$$

where

$$\beta_n = \frac{\frac{2n+1}{n}\varepsilon_e}{\epsilon_m(\omega) + \frac{n+1}{n}\varepsilon_e}. \tag{8}$$

When $n=1$, the electric field inside the MNP,

$$\tilde{\boldsymbol{E}}_{\text{MNP}} = s_\alpha \frac{1}{\varepsilon_{\text{eff}2} R_d^3} \left(\frac{\varepsilon_e}{\varepsilon_{\text{eff}1}} \tilde{\boldsymbol{p}} \right), \tag{9}$$

is just the electric field produced by the dipole inside the SQD at the point of the MNP's spherical center, i.e., the dipole approximation.

III. DENSITY MATRIX OF THE SYSTEM

In the SQD, we use a two-level exciton model to describe the optical process. The exciting laser field is now taken in the form $\boldsymbol{E}_0(t) = \tilde{\boldsymbol{E}}_0 \cos(\omega t)$. Under these conditions, the Hamiltonian is

$$H = \hbar\omega_0 a_2^\dagger a_2 - \chi(t)(a_2^\dagger a_1 + a_1^\dagger a_2), \tag{10}$$

where a_i and $a_i^\dagger$ are the annihilation and creation operators of level i $(i=1,2)$, corresponding to the vacuum ground state and the exciton state, respectively [see Fig. 1(b)]. Note that the energy of level 1 is taken as zero. $\chi(t) = \tilde{\chi} e^{-i\omega t} + \tilde{\chi}^* e^{i\omega t} = \boldsymbol{\mu} \cdot (\boldsymbol{E}_{\text{SQD}} + \boldsymbol{E}_{\text{SQD}}^*)$, where $\boldsymbol{\mu}$ is the interband optical transition matrix element. The excitation $\tilde{\chi}$ can be written as $\tilde{\chi} = \boldsymbol{\mu} \cdot (\tilde{\boldsymbol{E}}_1 + \tilde{\boldsymbol{E}}_2 + \tilde{\boldsymbol{E}}_3)$; the terms in this equation are defined by Eqs. (1)–(3).

These matrix elements satisfy the well-known optical Bloch equations,[27]

$$\partial_t \rho_{22} = \frac{i}{\hbar}\chi(t)[\rho_{21}^* - \rho_{21}] - \frac{1}{T_1}\rho_{22}, \tag{11}$$

$$\partial_t \rho_{21} = -i\omega_0 \rho_{21} + \frac{i\chi(t)}{\hbar}(1 - 2\rho_{22}) - \frac{1}{T_{20}}\rho_{21}. \tag{12}$$

Also, $\rho_{11} + \rho_{22} = 1$. T_1 and T_{20} are the longitudinal and transverse dephasing times. The dipole of the SQD relates to the interband polarization by $\boldsymbol{p} = \boldsymbol{\mu}(\rho_{21} + \rho_{21}^*)$, where $\rho_{21} = \langle a_1^\dagger a_2 \rangle$. In the rotating wave and steady state approximation, $\boldsymbol{p}(t) = \tilde{\boldsymbol{p}} e^{-i\omega t} + \tilde{\boldsymbol{p}}^* e^{i\omega t}$, where $\tilde{\boldsymbol{p}}$ is time independent. Then, the equations give

$$\rho_{22} = \frac{2T_1}{\hbar} \text{Im}[\tilde{\chi}^* \tilde{\rho}_{21}], \quad \tilde{\rho}_{21} = \frac{-\Omega\Delta}{(\omega - \omega_0 + G\Delta + i/T_{20})}, \tag{13}$$

where

$$\Omega = \frac{\boldsymbol{\mu} \cdot (\tilde{\boldsymbol{E}}_1 + \tilde{\boldsymbol{E}}_2)}{\hbar}, \tag{14}$$

$$G = \sum_{n=1}^{\infty} \frac{s_n \varepsilon_e \gamma_n R_0^{2n+1} \mu^2}{\varepsilon_{\text{eff}1}^2 R_d^{2n+4} \hbar} \equiv G_R + iG_I, \tag{15}$$

G_R and G_I are the real and imaginary parts of G, and $\Delta = \rho_{11} - \rho_{22}$. While Ω is determined by the electric field of $\tilde{\boldsymbol{E}}_1$ and $\tilde{\boldsymbol{E}}_2$, G totally comes from the contribution of the electric field $\tilde{\boldsymbol{E}}_3$, which is responsible for the interaction between a MNP and SQD. Therefore, the plasmon-exciton interaction leads to the formation of a hybrid exciton with shifted exci-

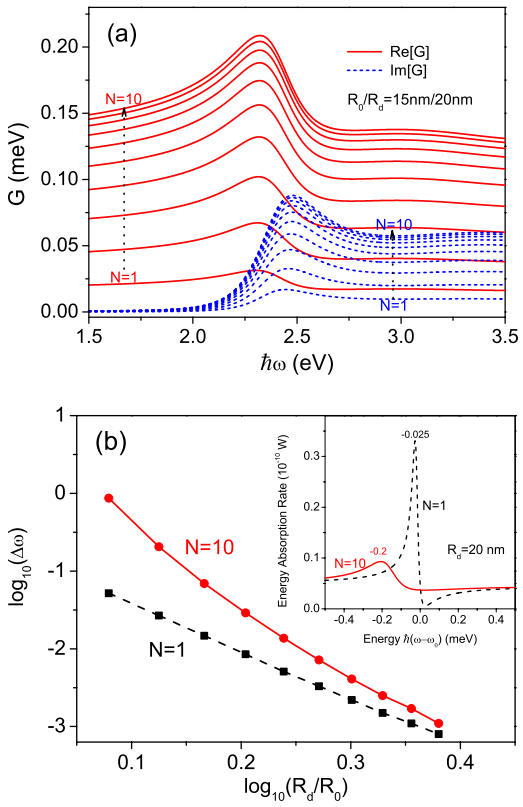

FIG. 2. (Color online) (a) The demonstration of multipole effect in system with MNP of Au. The solid (red) lines and dashed (blue) lines represent the real and imaginary parts of G, respectively. From bottom to top, N changes from 1 to 10. Radius of MNP and the distance are 15 and 20 nm, respectively. (b) Peak shift of energy absorption rate with different interparticle distances in logarithmic coordinate. The solid (red) line with circle is the one including multipole effect ($N=10$), while the dashed (black) line with square is only in dipole approximation ($N=1$). The inset is the contrast of energy absorption rate for a typical interparticle distance $R_d=20$ nm, with peak value emphasized.

ton frequency and decreased lifetime determined by G_R and G_I, respectively.

For a weak external field, $\Delta=\rho_{11}-\rho_{22}=1-2\rho_{22}\approx 1$ (since $\rho_{22}\ll 1$) and Eqs. (13) and (15) yield the solution of the problem. For a strong driving field, the problem is reduced to the nonlinear equation [Eq. (13)] investigated in Ref. 16. Since the quantity G_R includes multipole polarization in a MNP, the energy shift is determined by the multipole effect rather than a simple dipole effect. In Fig. 2(a), we plot $G=\Sigma_{n=1}^{N}(\cdots)$ with the change of frequency ω. The MNP is made of gold and the dielectric constant is taken from Ref. 28. Other parameters are chosen as $\varepsilon_s=6$, $R_0=15$ nm, and $R_d=20$ nm. The chosen SQD parameters are typical for the CdSe and CdTe colloidal quantum-dot systems. It shows that the excitonic frequency shift G_R enhances with N increasing and finally converges. Due to the factor $1/R_d^{2n+4}$, the terms of higher order have a smaller contribution. However, in the finite range, the contribution from terms of $n>1$ is more than that of $n=1$. The shift when $N=10$ is almost seven times that of $N=1$. $N=10$ is enough for convergence in all the cases studied in our paper. As for the lifetime of the exciton, it decreases with N increasing due to G_I. More close the distance of the molecule, more multipole contribution should be considered. In some case such as the frequency ω locates at the value making $\mathrm{Re}[\varepsilon_m(\omega)+3/2\varepsilon_e]=0$, the quadrupole effect becomes the leading one. As for the lifetime of the exciton, the interaction makes it shorter and multipole interaction boosts up this effect. For a Au MNP, the lifetime is almost unchanged when ω is below 2 eV, while the exciton frequency shift is still outstanding, which may have important applications.

The multipole effects can also be seen in the energy absorption spectrum. Under the radiation of a laser, both SQD and MNP absorb energy, which will be eventually transformed into heat by all kinds of scattering mechanics. The energy absorption rate is actually the time average of power dissipation density. In a SQD, the energy absorption rate Q_{SQD} is $Q_{\mathrm{SQD}}=\hbar\omega_0\rho_{22}/T_1$.

As for the MNP, the optical transmission property is more measured by the quantity of extinction, which has two main parts: absorption and scattering. The relative contribution of scattering to the extinction for metal particles of radius less than about 30 nm can be negligible. In the MNP-SQD molecules fabricated in recent experiments, the size of the MNP is within the range to discount the scattering. For example, the Rayleigh scattering has been calculated and found to be about 3 orders of magnitude smaller than the energy absorption rate.[16] The energy absorption rate in the MNP, Q_{MNP}, is expressed as $Q_{\mathrm{MNP}}=\frac{\omega}{2\pi}\int \mathrm{Im}[\varepsilon_m(\omega)]|\tilde{\boldsymbol{E}}_{\mathrm{MNP,tot}}|^2 dV$, where $\tilde{\boldsymbol{E}}_{\mathrm{MNP,tot}}=\frac{\varepsilon_e}{\varepsilon_{\mathrm{eff2}}}\frac{\tilde{\boldsymbol{E}}_0}{2}+\tilde{\boldsymbol{E}}_{\mathrm{MNP}}$ and $\tilde{\boldsymbol{E}}_{\mathrm{MNP}}$ is given by Eqs. (6)–(9). The total rate of absorption is therefore

$$Q_{\mathrm{tot}}=Q_{\mathrm{MNP}}+Q_{\mathrm{SQD}}. \tag{16}$$

A typical energy absorption spectrum is shown in the inset of Fig. 2(b). Here, the energy absorption rate including multipole effect for a typical value $R_d=20$ nm is plotted in contrast to the result in the dipole approximation in the inset. The interaction of the discrete state in the SQD and the continuous states in the MNP gives birth to the Fano line shape. The laser intensity is $I_0=1\ \mathrm{W/cm^2}$. The original excitonic energy is $\hbar\omega_0=2.5$ eV, i.e., the plasmon peak of Au. Figure 2 also plots the peak shift of the energy absorption rate with different interparticle distances in the weak field regime in logarithmic coordinate. With decreasing distance, the spectra has peak shifts and broadening. In the dipole approximation, the slope of the peak shift is -6 for $G\sim 1/R_d^6$; the multipole effect accounts for significant change in the relation of G and R_d and leads to the larger shift of peak. Especially when the value of R_d/R_0 is close to unity, the shift increases almost by 1 order of magnitude, which makes it more possible to be experimentally observed. As the interdistance of the molecule can be adjusted through biolinker by temperature, the shift is temperature controlled, which may have important application in sensor and detector. The broadening of the spectra is related to the incoherent energy transfer rate. The incoherent energy transfer in the hybrid molecule is via the Forster mechanism with energy transfer rate G_I. As the multipole effect increases the value of G_I in the vicinity of the

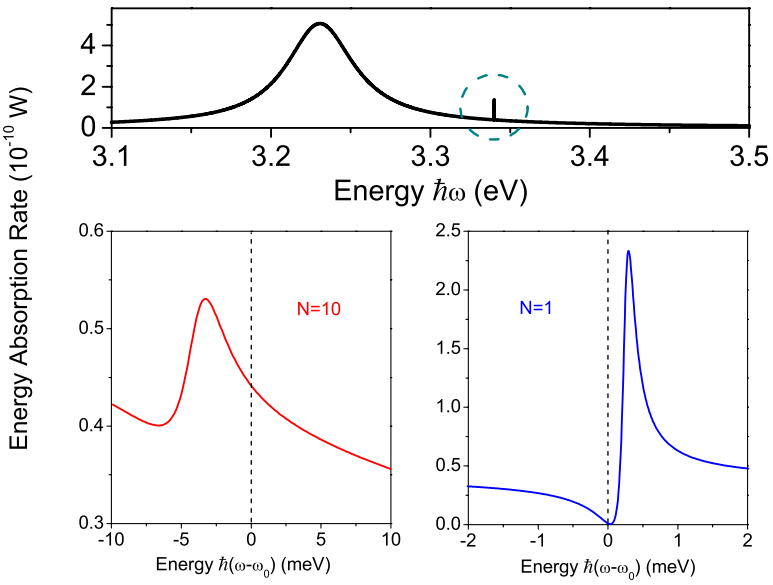

FIG. 3. (Color online) The different shifts caused by the multipole effect in contrast to dipole approximation. The Ag MNP and SQD are emerged in water ($\varepsilon_0=1.8$). Other parameters are $R_d=22$ nm, $R_0=15$ nm, and $\hbar\omega_0=3.34$ eV.

plasmon peak, see Fig. 2, the energy transfer time remarkably changes.

Multipole effects not only lead to quantitative changes (which is important for experiments) but also qualitative difference. For example, we consider the Ag MNP and SQD composed molecule emerged in water solution. As shown in Fig. 3, in the dipole approximation, the peak of a absorption rate has a blue shift. With the multipole effect, the peak's shift of the energy absorption rate changes to the red direction and the broadening increases a lot.

The total energy absorption versus interparticle distances for a fixed frequency is presented in Fig. 4, which shows that with decreasing the interparticle distance, the energy absorption first increases, then decreases. That means there exists an optimal distance for energy absorption. Here, the dipole approximation fails to provide the correct picture. The energy absorption of the MNP and SQD versus interparticle distance shows similar results (not shown here). The existence of optimal distance for SQD energy absorption can be understood in the following way. The energy absorption of the SQD depends on the competition of two factors: the local field enhancement and transfer the energy to MNP. With decreasing interparticle distance, local field becomes larger and energy transfer rate also increases. At short distance, the factor from fast energy transfer wins over the factor from local field enhancement. In fact, the Forster transfer (FT) rate is $1/\delta^3$; here, δ is the distance between the exciton and MNP surface ($\delta=R_d-R_0$).[12] When $\delta\to 0$, the FT rate $\to\infty$.

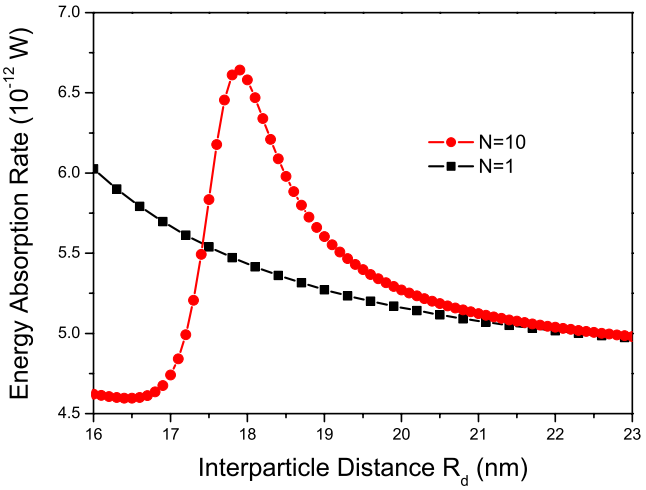

FIG. 4. (Color online) Total energy absorption versus interparticle distances for a fixed frequency $\hbar\omega=2.499$ eV. $R_0=15$ nm. Other parameters are the same as those for Fig. 2.

IV. ABSORPTION LINE SHAPES

By using Eqs. (13) and (16), we can write the absorption rate as

$$Q_{\rm tot}=Q^0_{\rm MNP}+\frac{A\bar{\Gamma}_{12}}{(\omega-\bar{\omega}_0)^2+\bar{\Gamma}^2_{12}}+\frac{B(\omega-\bar{\omega}_0)}{(\omega-\bar{\omega}_0)^2+\bar{\Gamma}^2_{12}}, \quad (17)$$

where $\bar{\Gamma}_{12}=1/T_{20}+G_I$ and $\bar{\omega}_0=\omega_0-G_R$ are the renormalized off-diagonal broadening and the modified absorption frequency, respectively. The absorption by an isolated MNP is given by $Q^0_{\rm MNP}=\frac{\omega}{8\pi}\,{\rm Im}[\varepsilon_m(\omega)]\left|\frac{\varepsilon_e E_0}{\varepsilon_{\rm eff2}}\right|^2 V_{\rm MNP}$, where $V_{\rm MNP}$ is the MNP volume. In the general case, the coefficients A and B are given by rather complex expressions. Here, it is instructive for us to give these coefficients in the dipole limit. Then, the key function G takes the form: $G=\frac{s_1\gamma_1\varepsilon_e R_0^3\mu^2}{\varepsilon^2_{\rm eff1}R_d^6\hbar}$. Note that $G_I>0$. For the limit $\Gamma_{12}\to 0$, we can obtain the Fano resonance,[20]

$$Q_{\rm tot}=Q^0_{\rm MNP}\frac{(\omega-\bar{\omega}_0-q_{\rm Fano}\Delta_{\rm int})^2}{(\omega-\bar{\omega}_0)^2+\Delta^2_{\rm int}}, \quad (18)$$

where $\Delta_{\rm int}=G_I$ is the interaction-induced broadening and $q_{\rm Fano}(\omega_0,d)=\frac{R_d^3}{s_\alpha R_0^3\,{\rm Im}[\gamma_1]}$ is the Fano factor. The line is strongly asymmetric if $q_{\rm Fano}(\omega_0,R_d)\sim 1$. In the limit $q_{\rm Fano}(\omega_0,R_d)\gg 1$, the absorption line becomes close to a Lorentzian. For molecular systems and systems at room temperature, the off-

diagonal decoherence is typically strong: $\Gamma_{12i} \gg |G|$. In this limit, the coefficients in the line shape become

$$A = \frac{\omega}{2\hbar}\left(\frac{\varepsilon_e \tilde{E}_0 \mu}{\varepsilon_{\text{eff1}}}\right)^2 \left|1 + \frac{s_\alpha \gamma_1 R_0^3}{R_d^3}\right| - \tilde{E}_0^2 \frac{\omega \mu^2 s_1 \varepsilon_e R_0^6 \,\text{Im}[\gamma_1]}{3\hbar \varepsilon_{\text{eff1}}^2 R_d^6} \left|\frac{\varepsilon_e}{\varepsilon_{\text{eff2}}}\right|^2 \text{Im}[\varepsilon_m(\omega)], \quad (19)$$

$$B = \frac{s_\alpha \mu^2 \varepsilon_e \tilde{E}_0^2 \omega R_0^3}{3\hbar \varepsilon_{\text{eff1}}^2 R_d^3} \text{Im}[\varepsilon_m(\omega)] \left|\frac{\varepsilon_e}{\varepsilon_{\text{eff2}}}\right|^2 \left(1 + \frac{s_\alpha R_0^3 \,\text{Re}[\gamma_1]}{R_d^3}\right). \quad (20)$$

In the strong decoherence regime, it is convenient to introduce an asymmetry factor,

$$q_{\text{asym}} = \frac{A}{B} = \frac{\frac{\varepsilon_e}{2}\left|1 + \frac{s_\alpha \gamma_1 R_0^3}{R_d^3}\right|^2 - \frac{s_1 R_0^6 \,\text{Im}[\gamma_1]}{3R_d^6}\left|\frac{\varepsilon_e}{\varepsilon_{\text{eff2}}}\right|^2 \text{Im}[\varepsilon_m(\omega)]}{\frac{s_\alpha R_0^3}{3R_d^3}\left|\frac{\varepsilon_e}{\varepsilon_{\text{eff2}}}\right|^2 \text{Im}[\varepsilon_m(\omega)]\left(1 + \frac{s_\alpha \,\text{Re}[\gamma_1] R_0^3}{R_d^3}\right)}.$$

If $|Q_{\text{asym}}| \sim 1$, the line shape is asymmetric and the interference effect is strong. We also should note that the interference effect may appear as a symmetric line with a dip. Such "antiresonance" may appear if $A < 0$ and $|q_{\text{asym}}| \gg 1$. The visibility of the antiresonance can be described by the ratio $|A/(\bar{\Gamma}_{12} Q^0_{\text{MNP}}(\omega_0)|$. Our numerical simulations show that antiresonances appear for small interparticle distances (see the graphs in the next section).

V. NUMERICAL RESULTS

In this section, we show the results of numerical calculations of energy absorptions for various systems. We pay special attention to the short interparticle distance regime, where the multipole effects are crucial. We emphasize the important role of the environment that is essential to describe and understand experiments. One of the effects of the environment is the dephasing time. Another is the dielectric constant of a matrix. These parameters have a significant impact on the asymmetric line shapes of an absorption spectrum.

In Fig. 5, we show the absorption spectrum of colloidal SQD-MNP(Au) for different interparticle distances. The parameters are $\hbar/T_{20}=1$ meV, $T_1=10$ ns, $R_0=10$ nm, $\varepsilon_e=1.8$ (water), and $\hbar\omega_0=2.356$ eV. The chosen dephasing times correspond to the low-temperature regime when the exciton broadening $\hbar/T_{20}=1$ meV is relatively small. One can see that the energy absorption spectrum has a symmetric peak for very large interparticle distance (100 nm), when the interparticle interaction is almost absent. With decreasing interparticle distance, an asymmetric Fano line shape appears due to the interaction between an exciton and plasmon.[16] From Fig. 5(b), we can see that with decreasing interparticle distance, the absorption spectrum shows quite different behaviors for small distance (strong interaction) and large distance (weak interaction) regimes. For large distance, we observe a blueshifted resonance, while for small distance, we see a redshifted antiresonance. The peak and/or valley intensity versus distance is show in Fig. 5(c). Overall, the interference features (asymmetry and antiresonance) become very

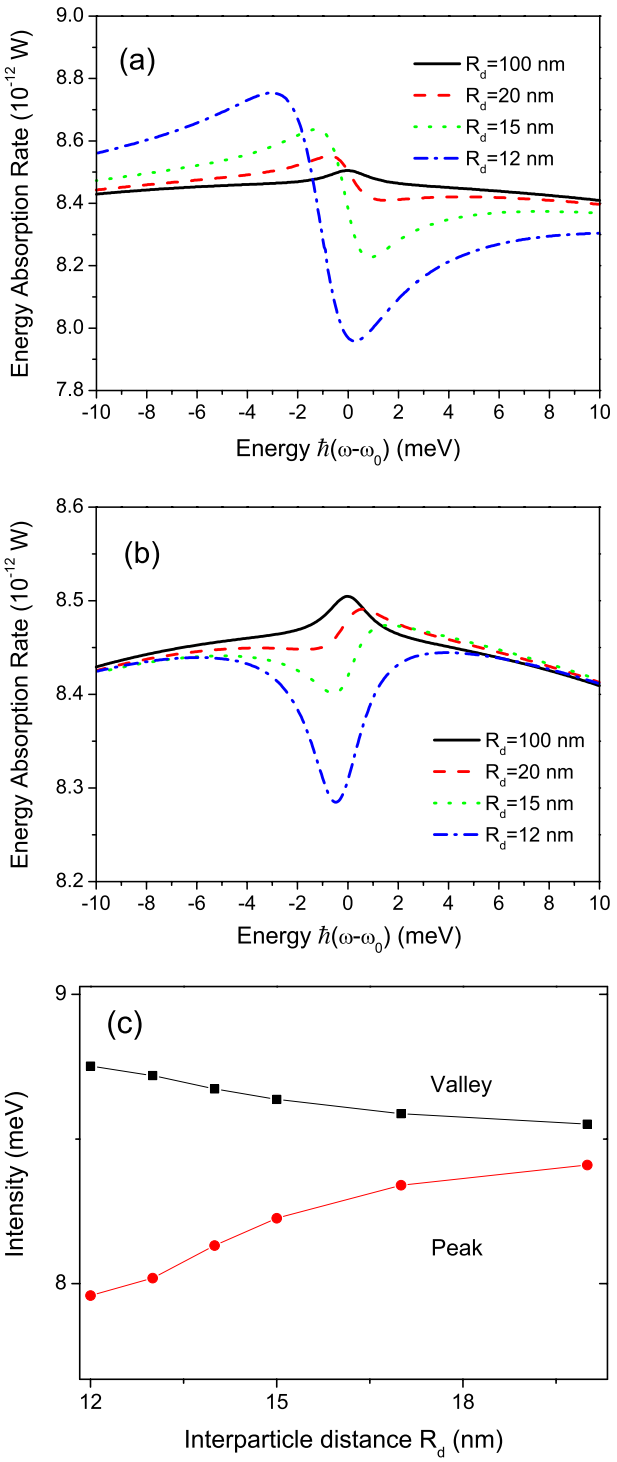

FIG. 5. (Color online) The absorption spectrum of SQD-MNP(Au). (a) Polarization is along the z direction. (b) Polarization is along the x direction. (c) The peak and valley intensities versus distance corresponding to (a).

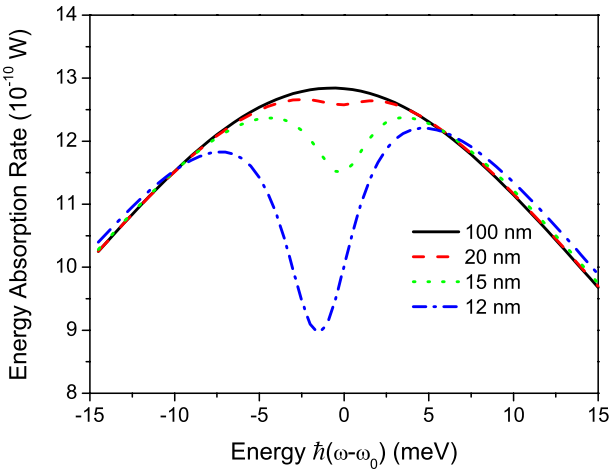

FIG. 6. (Color online) The absorption spectrum on epitaxial SQD- MNP(Au).

strong at small distances where the multipole effects govern the interparticle Coulomb interaction.

It is interesting to note that for large R_d (in Fig. 5), the exciton peak and MNP plasmon spectrum are constructively added, whereas for small R_d, we obtain destructive interference or antiresonance for the laser light along $\boldsymbol{x}$ or $\boldsymbol{y}$. For the laser light along $\boldsymbol{z}$, we see both strong constructive and destructive effects; however, the destructive dip is stronger. The physical origin of the destructive interference is in a reduction of absorption by the MNP (i.e., the term Q_{MNP} in the total absorption) due to the destructive interplay of external and induced electric fields. Regarding the absorption by the SQD (i.e., the term $Q_{\mathrm{SQD}} \propto \rho_{22}$), the integrated absorption by the SQD increases with decreasing R_d for $\tilde{\boldsymbol{E}}_0 \| \boldsymbol{z}$ and decreases with shortening R_d for $\tilde{\boldsymbol{E}}_0 \| \boldsymbol{x}(\boldsymbol{y})$. The reason is the dynamic screening of the external field inside the SQD by the MNP. Simultaneously, for short R_d, the exciton peak becomes shifted and strongly broadened.

In Fig. 6, we show the absorption spectrum of epitaxial SQD-MNP(Au) for different interparticle distances. The parameters are $\hbar/T_{20}=2$ meV, $T_1=T_{20}/2$, $R_0=10$ nm, $\varepsilon_e=\varepsilon_s=12$, the interband dipole matrix element $\mu=er_0$, $r_0=0.6$ nm, and $\hbar\omega_0=1.546$ eV. Again, the above parameters correspond to the low-temperature regime. The laser light polarization is taken as $\tilde{\boldsymbol{E}}_0 \| \boldsymbol{x}(\boldsymbol{y})$. In this case, we see line shapes with quite different Fano parameters compared to those for the colloidal SQD-MNP molecule. The minimum becomes very deep for two reasons: (1) Large background dielectric constant and, therefore, strong enhancement of electric fields inside the system and (2) the intrinsic exciton linewidth $1/T_{20}$ is relatively small and, therefore, the exciton-plasmon interaction becomes "concentrated" in a narrow energy interval. The above reasons (1 and 2) lead to a strong interference effect for the case shown in Fig. 6.

It is interesting that the visibility of the exciton in SQD-MNP molecules becomes greatly increased for small R_d (Figs. 5 and 6). This appears due to both the interference effect and plasmon enhancement. The plasmon enhancement effect is basically an increase of actual electric fields inside the system in the regime of exciton-plasmon and photon-plasmon resonances ($\omega_0 \approx \omega_{plasmon}$ and $\omega \approx \omega_{plasmon}$).[3,6,11] This effect of enhancement is often regarded as an antenna effect.[30,31] Mathematically, the plasmon enhancement appears in our equations through the factor $\frac{\epsilon_e}{\epsilon_m(\omega)}$. The typical enhancement factors for Au-based complexes with small R_d are about 10.[11,29] The increased visibility of the exciton resonance in a SQD-MNP molecule was also found for the dipole regime of interaction in Ref. 16. However, our present theory provides us with an exact solution for the electric fields and allows us to describe this effect for the most important regime of the multipole interaction. For example, the strong antiresonance in Fig. 5(b) is described by the factors $A/Q^0_{\mathrm{tot}} \approx 0.005$ and 0.02 for $R_d=100$ and 12 nm, respectively.

In the end of this section, we consider the spectra of hybrid complexes composed of optically active molecules and MNPs. An advantage of this system is that several or many dye molecules can be attached to a single MNP and, therefore, the interference effect can become much stronger.[7,17] Figure 7 shows the absorption spectrum of dye-MNP(Au) for different interparticle distances. The parameters correspond to the room-temperature regime and water environment: $\hbar/T_{20}=23$ meV, $T_1=5$ ns, and $\varepsilon_e=1.8\varepsilon_0$ (water). Other parameters are $R_0=10$ nm, $\mu=er_0$, $r_0=0.6$ nm, and $\hbar\omega_0=2.345$ eV. Here, we see that the environment has an important impact on the energy absorption. The very large off-diagonal decoherence leads again to quite different absorption line shapes. Importantly, even for the large room-temperature broadening (23 meV), we can see the antiresonance (left panel of Fig. 7). As it was shown in Sec. IV, the visibility of the antiresonance can be described by the ratio $|A/(\bar{\Gamma}_{12}Q^0_{\mathrm{MNP}}(\omega_0)|$. At high temperature, Γ_{12} becomes very large and the decoherence effects tend to reduce visibility of the antiresonance. Nevertheless, the antiresonance may survive even in the regime of a large broadening at room temperature (see left panel of Fig. 7). One sensitive method to observe the antiresonance can be to record the difference $Q_{\mathrm{tot}}-Q_{\mathrm{tot},initial}$, where Q_{tot} is the absorption by assembled complexes and $Q_{\mathrm{tot},initial}$ is the absorption by MNPs and QDs (dye molecules) before conjugation. The concrete conditions for the appearance of interference and antiresonance depend on the system details and environment.

The depth of antiresonance can be enhanced by attaching few or many dye molecules. By neglecting the interaction between dye molecules and the dipole orientation, we can write $A_N=NA$, where A_N is the antiresonance coefficient for the N-molecule complex, A is the coefficient for a single dye molecule, and N is the number of attached dye molecules. Correspondingly, the depth of the antiresonance of the N-molecule complex becomes $|\Delta Q_N|=N|\Delta Q|$, where ΔQ is depth of the antiresonance for a single dye molecule. The above dependence $\Delta Q \propto N$ is valid if the interaction between excitons is weaker than the exciton-MNP coupling. The strength of the exciton-exciton interaction is proportional to $1/d^3$, where d is the distance between two neighboring dye molecules. This distance can be estimated as $\sqrt{S/N}$, where $S=4\pi R_0^2$ is the surface area of a MNP. Simultaneously, the exciton-MNP interaction energy is proportional to $1/\delta^3$ (see Sec. III). Therefore, if N is not too large, the exciton-exciton

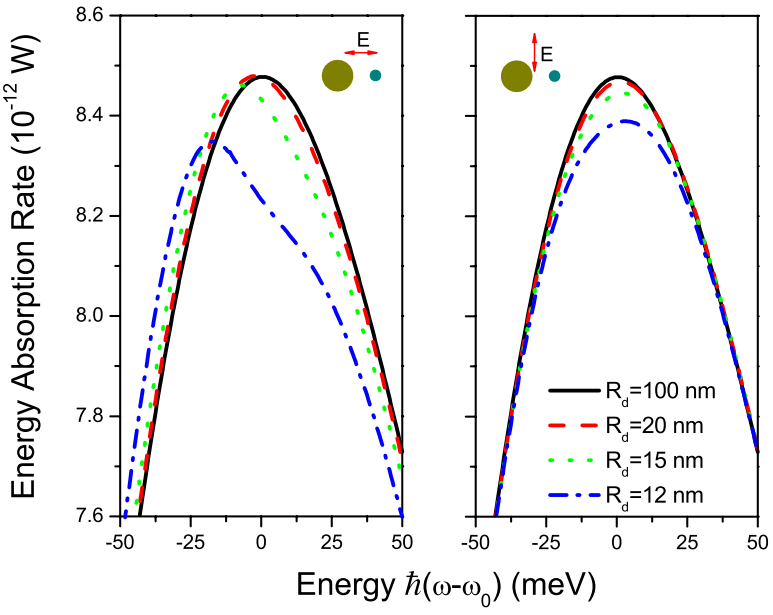

FIG. 7. (Color online) The absorption spectrum of a dye-MNP complex. The dipole is parallel (left) and perpendicular (right) to the MNP surface

interaction can be neglected if $\delta \ll R_0$. From Fig. 7, we see that the effect of the single exciton antiresonance on the total absorption spectrum $|\Delta Q|/Q^0_{\mathrm{MNP}} \approx 0.035\%$ or 3.5%. If we now assume a structure with $N=10$, we obtain $|\Delta Q_N|/Q^0_{\mathrm{MNP}} \approx 35\%$. This tells us that the change in the total absorption spectrum due to the exciton-plasmon antiresonance can be experimentally seen.

VI. CONCLUSION

We investigate the optical properties of hybrid molecules composed of a SQD, dye, and MNPs. The main focus of the paper is the regime of strong exciton-plasmon interaction and multipole effects. First, we derive an exact analytical solution for electric fields and absorption spectra. Then, we show that the multipole effects play the crucial role for the strong interaction regime. When the interparticle distance is relatively small, the multipole effect significantly gives larger peak shifts and broadenings for the energy absorption rate and the dipole approximation fails. The results obtained in this paper can be used to analyze optical experiments on hybrid systems with a strong exciton-plasmon interaction.

ACKNOWLEDGMENTS

This work is supported in part by the National Natural Science Foundation of China under Grants Nos. 10574017 and 10774016 and by a grant of the China Academy of Engineering and Physics. A.O.G. thanks the NSF and BNNT Initiative at Ohio University for financial support.

*zhang_wei@iapcm.ac.cn
†govorov@helios.phy.ohiou.edu

[1] Y. Cui, Q. Wei, H. Park, and C. M. Lieber, Science **293**, 1289 (2001).
[2] Y. Yin, C. Erdonmez, and A. P. Alivisatos, Nature (London) **437**, 664 (2005).
[3] C. D. Geddes and J. R. Lakowicz, J. Fluoresc. **12**, 121 (2002).
[4] K. T. Shimizu, W. K. Woo, B. R. Fisher, H. J. Eisler, and M. G. Bawendi, Phys. Rev. Lett. **89**, 117401 (2002).
[5] P. Anger, P. Bharadwaj, and L. Novotny, Phys. Rev. Lett. **96**, 113002 (2006).
[6] J. Lee, A. O. Govorov, J. Dulka, and N. A. Kotov, Nano Lett. **4**, 2323 (2004); J. Lee, T. Javed, T. Skeini, A. O. Govorov, G. W. Bryant, and N. A. Kotov, Angew. Chem. **45**, 4819 (2006).
[7] N. G. Liu, B. S. Prall, and V. I. Klimov, J. Am. Chem. Soc. **128**, 15362 (2006).
[8] E. W. Edwards, D. Y. Wang, and H. Mohwald, Macromol. Chem. Phys. **208**, 439 (2007); G. Lu, H. Shen, B. Cheng, Z. Chen, C. A. Marquette, L. J. Blum, O. Tillement, S. Roux, G. Ledoux, M. Ou, and P. Perriat, Appl. Phys. Lett. **89**, 223128 (2006).
[9] Y. Ito, K. Matsuda, and Y. Kanemitsu, Phys. Rev. B **75**, 033309 (2007); V. K. Komarala, Y. P. Rakovich, A. L. Bradley, S. J. Byrne, Y. K. Gunko, N. Gaponik, and A. Eychmller, Appl. Phys. Lett. **89**, 253118 (2006).
[10] J. M. Slocik, A. O. Govorov, and R. R. Naik, Supramol. Chem. **18**, 415 (2006).
[11] A. O. Govorov, G. W. Bryant, W. Zhang, T. Skeini, J. Lee, N. A. Kotov, J. M. Slocik, and R. R. Naik, Nano Lett. **6**, 984 (2006).
[12] B. N. J. Persson and N. D. Lang, Phys. Rev. B **26**, 5409 (1982).
[13] H. T. Dung, L. Knoll, and D.-G. Welsch, Phys. Rev. A **62**, 053804 (2000); G. S. Agarwal and S. V. O'Neil, Phys. Rev. B **28**, 487 (1983).
[14] V. V. Klimov, M. Ducloy, and V. S. Letokhov, Phys. Rev. A **59**, 2996 (1999).
[15] Th. Förster, in *Modern Quantum Chemistry*, edited by O. Sinanoglu (Academic, New York, 1965).

[16] W. Zhang, A. O. Govorov, and G. W. Bryant, Phys. Rev. Lett. **97**, 146804 (2006).
[17] A. M. Kelley, Nano Lett. **7**, 3235 (2007).
[18] D. Neuhauser and K. Lopata, J. Chem. Phys. **127**, 154715 (2007).
[19] M.-T. Cheng, S.-D. Liu, H.-J. Zhou, Z.-H. Hao, and Q.-Q. Wang, Opt. Lett. **32**, 2125 (2007).
[20] U. Fano, Phys. Rev. **124**, 1866 (1961).
[21] D. C. Driscoll, M. P. Hanson, A. C. Gossard, and E. R. Brown, Appl. Phys. Lett. **86**, 051908 (2005).
[22] U. Woggon, E. Herz, O. Schops, M. V. Artemyev, Ch. Arens, N. Rousseau, D. Schikora, K. Lischka, D. Litvinov, and D. Gerthsen, Nano Lett. **5**, 483 (2005).
[23] Yu. I. Mazur, W. Q. Ma, X. Wang, Z. M. Wang, G. J. Salamo, M. Xiao, T. D. Mishima, and M. B. Johnson, Appl. Phys. Lett. **83**, 987 (2003); J. H. Lee, Z. M. Wang, K. Sablon, and G. J. Salamo, Cryst. Growth Des. **8**, 690 (2008).
[24] L. D. Landau and E. M. Lifshitz, *Electrodynamics of Continuous Media* (Pergamon, Oxford, 1960).
[25] G. Mie, Ann. Phys. **25**, 377 (1908).
[26] K. L. Kelly, E. Coronado, L. L. Zhao, and G. C. Schatz, J. Phys. Chem. B **107**, 668 (2003).
[27] H. Haug and S. W. Koch, *Quantum Theory of the Optical and Electronic Properties of Semiconductors*, 4th ed. (World Scientific, Singapore, 2004).
[28] P. B. Johnson and R. W. Christy, Phys. Rev. B **6**, 4370 (1972).
[29] A. O. Govorov and I. Carmeli, Nano Lett. **7**, 620 (2007).
[30] R. Baer, D. Neuhauser, and S. Weiss, Nano Lett. **4**, 85 (2004).
[31] S. Nie and S. R. Emory, Science **275**, 1102 (1997).